

VVTRec: Radio Interferometric Reconstruction through Visual and Textual Modality Enrichment

Kai Cheng¹, Ruoqi Wang² and Qiong Luo^{*,1,2}

¹The Hong Kong University of Science and Technology

²The Hong Kong University of Science and Technology (Guangzhou)

kai.cheng@connect.ust.hk, rwang280@connect.hkust-gz.edu.cn, luo@ust.hk

Abstract

Radio astronomy is an indispensable discipline for observing distant celestial objects. Measurements of wave signals from radio telescopes, called visibility, need to be transformed into images for astronomical observations. These dirty images blend information from real sources and artifacts. Therefore, astronomers usually perform reconstruction before imaging to obtain cleaner images. Existing methods consider only a single modality of sparse visibility data, resulting in images with remaining artifacts and insufficient modeling of correlation. To enhance the extraction of visibility information and emphasize output quality in the image domain, we propose VVTRec, a multimodal radio interferometric data reconstruction method with visibility-guided visual and textual modality enrichment. In our VVTRec, sparse visibility is transformed into image-form and text-form features to obtain enhancements in terms of spatial and semantic information, improving the structural integrity and accuracy of images. Also, we leverage Vision-Language Models (VLMs) to achieve additional training-free performance improvements. VVTRec enables sparse visibility, as a foreign modality unseen by VLMs, to accurately extract pre-trained knowledge as a supplement. Our experiments demonstrate that VVTRec effectively enhances imaging results by exploiting multimodal information without introducing excessive computational overhead.

1 Introduction

In radio astronomy, *visibility* refers to the complex data measured in the *uv-plane* by radio interferometers, representing the cross-correlation between pairs of antenna signals. It characterizes the distribution of the sky in the frequency domain and serves as the source for interferometric imaging. Images directly transformed from such visibility data are called *dirty images*, because they differ significantly from the real sky [Högbom, 1974; Ables, 1974; Bouman *et al.*, 2016;

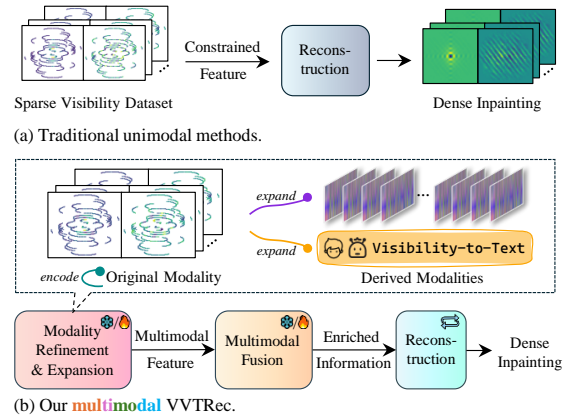


Figure 1: Comparison of traditional unimodal visibility data processing paradigm and our multimodal pipeline.

Connor *et al.*, 2022]. This discrepancy arises due to artifacts and various other factors [Schmidt *et al.*, 2022]. On the one hand, visibility data are inherently sparse. Due to limitations in telescope configurations, the data are distributed only along a small number of trajectories, leaving most spatial frequency regions unmeasured. On the other hand, phenomena such as cosmic microwave background, galactic radiation, atmospheric disturbances, and receiver interferences introduce additional radio noise [Wilson, 1979; Singh *et al.*, 2022]. Consequently, visibility data typically require reconstruction before subsequent scientific studies. In this paper, we propose a reconstruction method that enhances imaging quality by exploiting multimodal information.

The first challenge in visibility data reconstruction lies in the inherently limited information in sparse visibility. As shown in Figure 1(a), sparse visibility is a weak signal whose distribution on the uv-plane is non-uniform and exhibits certain discreteness. This sparsity and context insufficiency render constrained features. However, downstream reconstructions in previous unimodal methods solely rely on the information provided by visibility, which makes it challenging to predict as many blank spatial regions as possible while maintaining prediction accuracy based on a small number of known signal locations.

The second challenge is that current strategies can only

*Corresponding Author.

exploit unimodal complex-valued visibility, leading to some defects in reconstructed images. For example, structural information about images or semantic context cannot be adequately derived from this single modality of sparse visibility alone. Furthermore, relying solely on unimodal sparse visibility underestimates the interplay between the frequency and final target image domains [Zhao *et al.*, 2025b], reducing the reconstruction quality. Moreover, previous methods often ignore explicit spatial modeling in the unimodal setting [Schmidt *et al.*, 2022; Wang *et al.*, 2024; Wang *et al.*, 2025], leading to further limitations in their ability to extract spatial correlations. This makes a relatively negative impact on final imaging results.

To overcome these challenges, we propose VVTRec, a radio interferometric data reconstruction approach that turns sparse astronomical observations into visibility-guided visual and textual modality enrichment. Leveraging external knowledge as a supplement is beneficial, further necessitating multimodal enhancements. As shown in Figure 1 (b), through modality expansion, our VVTRec designs transformations based on the characteristics of sparse visibility, converting visibility into image-form and text-form modalities. The image-form modality is a generated feature map of visibility data to explicitly enhance spatial information. The text-form modality provides dataset-level and sample-level descriptions of visibility data to supplement semantic information. The three modalities collectively provide multiple sources for reconstruction, enabling access to richer underlying information and pretrained knowledge.

Both derived modalities are designed to address the issue of integrating external knowledge since visibility is foreign to pretrained models. Based on the perspective of the belief network, we propose a knowledge bank that uses encoded visibility as the query to perform the integration and selection of multimodal external knowledge in a sample-specific manner. The generated image-form modality preserves key features from visibility while also introducing an image structure. Specifically, previous methods involve the image domain only in the final imaging step, whereas our VVTRec establishes connections between the two domains at the beginning of the process. Meanwhile, the text-form modality also provides rich textual descriptions, enabling visibility to extract contextual features.

By leveraging the pre-trained knowledge of Visual-Language Models (VLMs) [Zhang *et al.*, 2025; Zhong *et al.*, 2025; Zhao *et al.*, 2025a], VVTRec performs joint modeling across modalities seamlessly within a unified space and further enhances the performance. It is highly compatible with current pretrained models [Kim *et al.*, 2021; Radford *et al.*, 2021; Li *et al.*, 2023; Xue *et al.*, 2025]. For sparse visibility, the pre-trained knowledge within VLMs represents two foreign modalities. Similarly, for VLMs, visibility itself is also a foreign modality. Therefore, VVTRec exploits their dependencies and enables the transformed modalities to effectively extract proper external complementary knowledge from pre-trained models. Notably, VVTRec focuses on fully utilizing existing pre-trained knowledge to achieve performance gains. Additionally, VVTRec incurs little additional computational overhead or causes speed drops

sharply when incorporating more modalities. In other words, VVTRec enhances model performance while maintaining efficiency.

Overall, our contributions can be summarized as follows:

- We propose VVTRec to transform sparse visibility into expanded modalities to enhance spatial and semantic information extraction, addressing challenges in radio interferometric data reconstruction.
- We propose a sample-specific knowledge bank to leverage and fuse external pre-trained knowledge for improved reconstruction by joint modeling of mutually foreign modalities into multimodal features.
- VVTRec can gain training-free performance improvements, and experimental results show that it successfully enhances reconstructions across different datasets with little additional computational overhead.

2 Background and Related Work

2.1 Radio Interferometric Imaging

Radio telescopes offer many unique advantages for observing the universe within the radio transmission windows. They can penetrate interstellar dust and reveal the internal structures [Steyn *et al.*, 2024]. Additionally, they provide insights into unique physical mechanisms [Xu *et al.*, 2022; Collaboration *et al.*, 2022]. They can also form a virtual Earth-sized telescope through Very Long Baseline Interferometry (VLBI) [Bouman *et al.*, 2018]. However, limited baselines are one of the main reasons for the sparsity of visibility data [Thompson *et al.*, 2017; Bouman *et al.*, 2018], highlighting the importance of designing algorithms for reconstruction.

While visibility data represented in the uv-plane facilitates signal processing operations, it is unsuitable for intuitive observations. By applying the Inverse Fourier Transform (IFT) [Jin *et al.*, 2025], frequency-domain features can be remapped back into the image domain, which can later be studied visually [Wang *et al.*, 2023]. The imaging process of the spatial intensity distribution is represented as follows:

$$I(l, m) = \int_u \int_v \mathcal{M}(u, v) e^{j2\pi(ul+vm)} du dv, \quad (1)$$

where $\mathcal{M}(u, v)$ denotes the frequency-domain visibility data and $I(l, m)$ denotes the intensity distribution of the sky.

2.2 Interferometric Data Reconstruction

Radio interferometric imaging inherently constitutes an ill-posed inverse problem due to the sparse sampling in the uv-plane, while direct imaging results in severe artifacts [Wang *et al.*, 2025]. Traditional methods address this by iteratively removing artifacts to obtain *clean images*. The CLEAN algorithm [Cornwell, 2008] iteratively removes the dirty beam in the image domain. This approach aims to overcome the ambiguity caused by incomplete data by suppressing coherent interference. However, the assumption of point-like sources in CLEAN results in unrealistic reconstructions for other types of sources [Connor *et al.*, 2022]. Furthermore, the iterative method of CLEAN can lead to a long inference time.

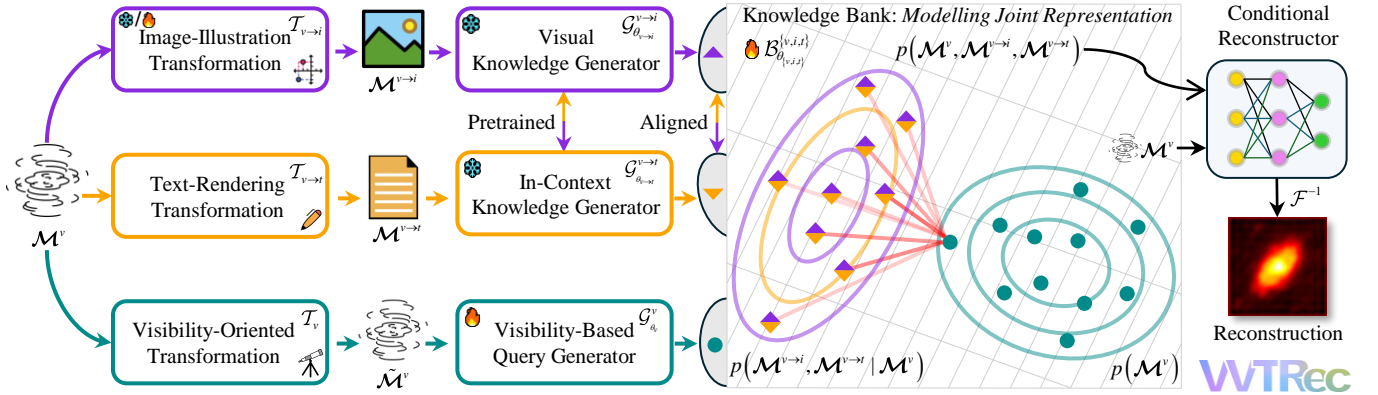


Figure 2: Overview of our proposed method VVTRec. It consists of four key components: (1) The transformations provide essential modality refinement and expansion for viewing visibility data from a multimodal perspective. (2) The generators encode rich and consistent information from three modalities into latent spaces for further alignment and extraction. (3) The knowledge bank retrieves the enriched multimodal features in a unified space by modelling the joint distribution of all modalities. (4) The conditional reconstructor is designed to combine extracted features into the reconstruction and imaging process.

Recently, some learning-based approaches have made advances by focusing on the reconstruction of visibility data. Early methods utilized dirty images to make major contributions to the conversion into clean images, regardless of the noise before imaging [Bouman *et al.*, 2016; Connor *et al.*, 2022]. However, reconstructing visibility data is later demonstrated to be more effective than image reconstruction and becomes the prevailing choice. Specifically, Schmidt *et al.* [Schmidt *et al.*, 2022] introduced convolutional neural network models for reconstructing incomplete data in radio imaging. Wu *et al.* [Wu *et al.*, 2022] proposed a method to embed visibility measurements into input tokens by exploring their features in the hidden space. Wang *et al.* [Wang *et al.*, 2024] introduced a radial visibility loss to consider all components in the angular coordinates. Wang *et al.* also [Wang *et al.*, 2025] explored supervised and self-supervised learning of interferometric image reconstruction. In comparison to existing work, our VVTRec is capable of effectively exploiting multimodal knowledge by integrating external knowledge to supplement sparse visibility and boost reconstruction performance.

3 Methodology

3.1 Overall Architecture

The overall framework of VVTRec is depicted in Figure 2. \mathcal{M}^v denotes sparse visibility and is defined as:

$$\mathcal{M}^v = \mathbf{D}_\Lambda \mathcal{F}(\mathbf{x}) + \epsilon, \quad (2)$$

where \mathbf{x} is the corresponding image, \mathcal{F} is the Fourier transformation and ϵ represents the noise. \mathbf{D}_Λ is an under-sampling matrix where Λ denotes telescopes' sampling pattern. The image-illustration transformation $\mathcal{T}_{v \rightarrow i} : \Omega_{\text{freq}} \mapsto \Omega_{\text{spatial}}$ and text-rendering transformation $\mathcal{T}_{v \rightarrow t} : \Omega_{\text{freq}} \mapsto \Omega_{\text{semantic}}$ are employed to produce the essential image-form modality $\mathcal{M}^{v \rightarrow i}$ and text-form modality $\mathcal{M}^{v \rightarrow t}$ of visibility data. A visibility-oriented transformation is also utilized to refine the encoding of visibility modality \mathcal{M}^v , outputting $\tilde{\mathcal{M}}^v$. On the

one hand, these modalities are different in form, and each provides distinct and rich information. On the other hand, they are all rooted in the same source and collaboratively represent visibility data. Thus, we utilize generators to encode information from three modalities into latent spaces for further knowledge alignment and extraction. Specifically, $\mathcal{G}_{\theta_{v \rightarrow i}}^v$, $\mathcal{G}_{\theta_{v \rightarrow t}}^v$, and $\mathcal{G}_{\theta_v}^v$ denote the Visual Knowledge Generator (VKG), In-context Knowledge Generator (IKG), and Visibility Query Generator (VQG), respectively. To facilitate the smooth fusion between the vision-language domain and interferometric frequency domain, we adopt the Transformer encoder [Vaswani *et al.*, 2017] to establish VQG. We omit the subscripts for parameters in these notations for simplicity. Subsequently, the Knowledge Bank (KB) retrieves the enriched multimodal features in a unified space by modelling the joint distribution of all modalities. The Conditional Reconstructor (CR) is designed to combine extracted features and facilitate the reconstruction and imaging. Overall, our architecture enables effective information fusion from foreign modalities to boost the radio interferometric data reconstruction. Pre-trained knowledge is therefore sufficiently utilized, and a considerable number of parameters can be frozen without introducing excessive computational overhead. Moreover, datasets used in pre-trained models [Kim *et al.*, 2021; Radford *et al.*, 2021; Li *et al.*, 2023; Xue *et al.*, 2025] do not contain content in the field of radio interferometry, further ensuring the effectiveness and generalization.

3.2 Modality Transformation

Modelling visibility data from a multimodal view is beneficial for reconstruction from sparse visibility. Transforming visibility into more types of modalities in compliance with the input requirements of pre-trained models is vital. Visibility data are discrete signals with strong astronomical significance, which are formalized in the frequency domain. Thus, our VVTRec takes into account both the preservation of astronomical information and the transformation of modal forms. The steps of the image-illustration transformation $\mathcal{T}_{v \rightarrow i}$ can

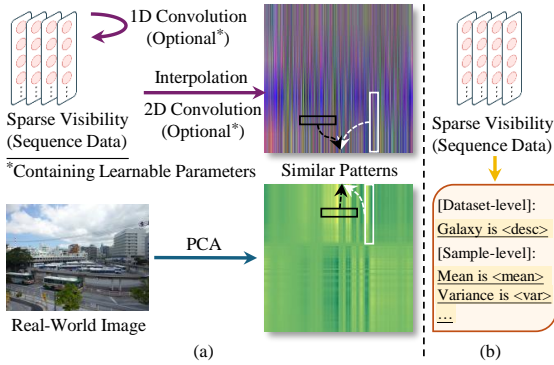


Figure 3: (a) Comparison of the generated image-form feature map and PCs of an image in the pretraining dataset [Lin *et al.*, 2014]. (b) An example of retrieving in-context information from sparse visibility.

be formulated as follows:

$$\mathcal{M}^{v \rightarrow i} = \text{Conv}_{\theta_{c,2}}^{2D} \left(\mathcal{I} \left(\text{Conv}_{\theta_{c,1}}^{1D} (\mathcal{M}^v) \right) \right), \quad (3)$$

where Conv^{1D} and Conv^{2D} are optional 1D and 2D convolutions, respectively. \mathcal{I} is the interpolation operation. The rationale behind $\mathcal{T}_{v \rightarrow i}$ is also shown in Figure 3 (a). We sample an image of the dataset [Lin *et al.*, 2014] used for VLM pretraining and further process it by Principal Component Analysis (PCA). The key observations are the similar patterns in our generated image-form feature map and the visualization of PCs, suggesting that VLM has the potential to extract information from sparse visibility data within our proposed framework. Moreover, to better leverage the pre-trained ability in the aligned vision-language space, we also extract the in-context information from sparse visibility as shown in Figure 3 (b). At the dataset level, entities such as research subjects and metadata are briefly described. At the sample level, statistics are calculated as part of the prompt as well. It enables external knowledge to supplement the prior of reconstruction with semantic information.

3.3 Enrichment from Sample-Specific Knowledge

As shown in Figure 2, the visual and textual modalities $\{\mathcal{M}^{v \rightarrow i}, \mathcal{M}^{v \rightarrow t}\}$ are both derived from the visibility modality \mathcal{M}^v , implying their dependent relationships. We can formulate the goal of our KB $\mathcal{B}^{\{v,i,t\}}$ as modelling the joint representation $p(\mathcal{M}^{v \rightarrow i}, \mathcal{M}^{v \rightarrow t}, \mathcal{M}^v)$. However, directly obtaining this joint representation is challenging. We observe that a directed acyclic graph naturally formed in modality expansion can help ease the modelling if we split this joint representation as two parts from the perspective of a belief network, as follows:

$$p(\mathcal{M}^{v \rightarrow i}, \mathcal{M}^{v \rightarrow t}, \mathcal{M}^v) = p(\mathcal{M}^{v \rightarrow i}, \mathcal{M}^{v \rightarrow t} | \mathcal{M}^v) p(\mathcal{M}^v). \quad (4)$$

Both VKG $\mathcal{G}^{v \rightarrow i}$ and IKG $\mathcal{G}^{v \rightarrow t}$ can exploit modalities $\mathcal{M}^{v \rightarrow i}$ and $\mathcal{M}^{v \rightarrow t}$ well, as they are already aligned in the feature space during the pretraining of VLM. This is another design advantage of VVTRec in addition to the training-free gain, since it can skip training on the conditional joint representation of $\mathcal{M}^{v \rightarrow i}$ and $\mathcal{M}^{v \rightarrow t}$. Thus, we define

$\xi_{\mathcal{M}^{v \rightarrow i}, \mathcal{M}^{v \rightarrow t} | \mathcal{M}^v}$ to represent $p(\mathcal{M}^{v \rightarrow i}, \mathcal{M}^{v \rightarrow t} | \mathcal{M}^v)$ as follows:

$$\xi_{\mathcal{M}^{v \rightarrow i}, \mathcal{M}^{v \rightarrow t} | \mathcal{M}^v} = \mathcal{A}(\mathcal{G}^{v \rightarrow i}(\mathcal{M}^{v \rightarrow i}), \mathcal{G}^{v \rightarrow t}(\mathcal{M}^{v \rightarrow t})), \quad (5)$$

where $\mathcal{A}(\alpha, \beta) = \alpha || \beta$ is the concatenation operation. Moreover, we can define $\zeta_{\mathcal{M}^v}$ from the output of VQG \mathcal{G}^v to serve as the latent representation of $p(\mathcal{M}^v)$, which can be formulated as:

$$\zeta_{\mathcal{M}^v} = \mathcal{G}^v(\mathcal{M}^v). \quad (6)$$

Based on $\xi_{\mathcal{M}^{v \rightarrow i}, \mathcal{M}^{v \rightarrow t} | \mathcal{M}^v}$ and $\zeta_{\mathcal{M}^v}$, we can obtain the latent representation of $p(\mathcal{M}^{v \rightarrow i}, \mathcal{M}^{v \rightarrow t}, \mathcal{M}^v)$ as follows:

$$\eta_{\{v,i,t\}} = \mathcal{B}^{\{v,i,t\}}(\xi_{\mathcal{M}^{v \rightarrow i}, \mathcal{M}^{v \rightarrow t} | \mathcal{M}^v}, \zeta_{\mathcal{M}^v}). \quad (7)$$

To fully capture the underlying characteristics and correlations of modalities, we design KB to obtain effective multimodal features with enriched information to facilitate reconstruction, as shown in Figure 4. For VKG and IKG, \mathcal{M}^v is a foreign modality and inapplicable to direct process. After VVTRec employs the transformations, VKG and IKG are able to leverage their pre-trained ability to exploit the expanded modalities with knowledge passed from visibility. The resulting $\xi_{\mathcal{M}^{v \rightarrow i}, \mathcal{M}^{v \rightarrow t} | \mathcal{M}^v}$ can be viewed as a pool of enriched knowledge with respect to the original astronomical signals. Moreover, KB has a different instance for each sample as it is automatically updated in a sample-specific manner. Thus, we use each $\zeta_{\mathcal{M}^v}$ as the query and its corresponding $\xi_{\mathcal{M}^{v \rightarrow i}, \mathcal{M}^{v \rightarrow t} | \mathcal{M}^v}$ as the KB and perform the feature selection and integration. Specifically, we first perform the crossmodal attention to aggregate the effective portions of KB. A single head is formulated as:

$$\kappa^{h_j} = \text{softmax} \left(\frac{\xi_{\mathcal{M}^{v \rightarrow i}, \mathcal{M}^{v \rightarrow t} | \mathcal{M}^v}^{h_j} \cdot \xi_{\mathcal{M}^v}^{h_j}}{\sqrt{d_\xi}} \right) \xi_{\mathcal{M}^{v \rightarrow i}, \mathcal{M}^{v \rightarrow t} | \mathcal{M}^v}^{h_j}, \quad (8)$$

where h_j is the j -th head of the crossmodal attention and d_ξ is the dimension of $\xi_{\mathcal{M}^{v \rightarrow i}, \mathcal{M}^{v \rightarrow t} | \mathcal{M}^v}$. Then, the calculation of multimodal $\eta_{\{v,i,t\}}$ is finalized by fusing the retrieved knowledge κ and $\zeta_{\mathcal{M}^v}$ using the residual connection as follows:

$$\eta_{\{v,i,t\}} = \kappa(\zeta_{\mathcal{M}^v}) + \zeta_{\mathcal{M}^v}. \quad (9)$$

3.4 Conditional Reconstructor

In terms of the reconstruction process, we also only utilize the sparse visibility as the input and a neural field to fulfill the constraints of the mapping following the setting of Wu *et al.* [Wu *et al.*, 2022]. To make this process trainable together

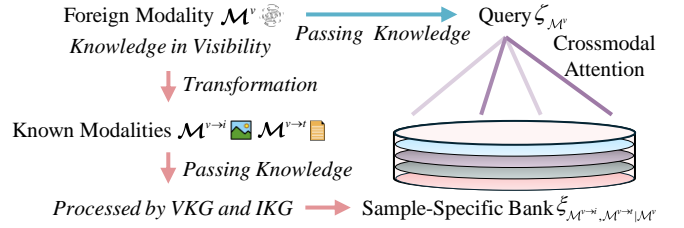


Figure 4: Illustration of the workflow of the sample-specific knowledge bank, along with the knowledge pass and integration.

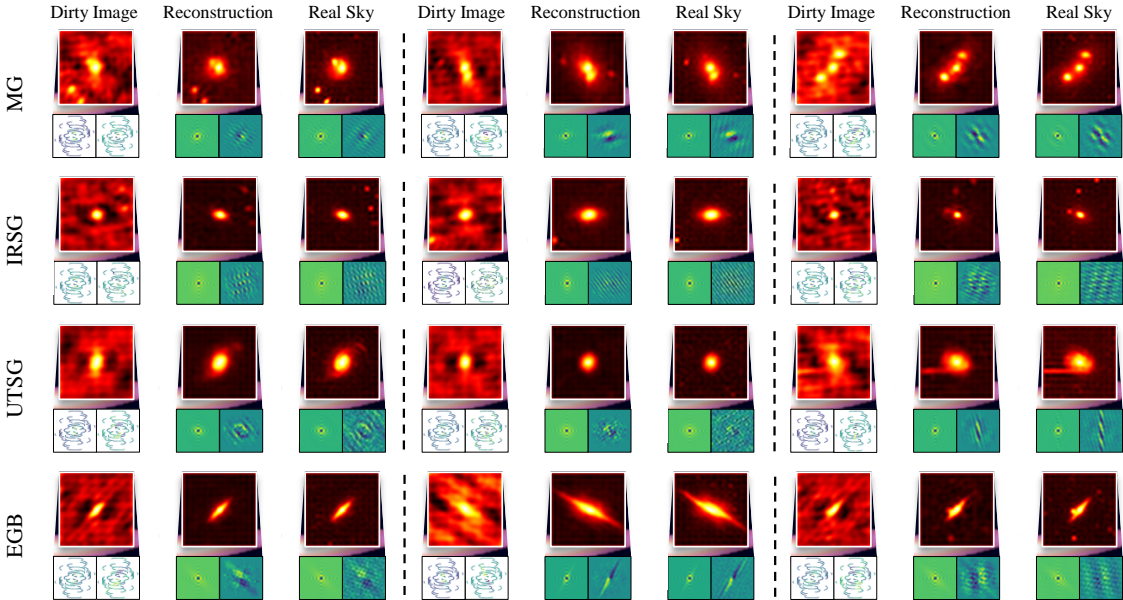


Figure 5: Visualization of the reconstruction results of VVTRec compared with the dirty image and real sky, including both visibility and image. The left half of the panel below is the real part, and the right half is the imaginary part.

with the other modules of VVTRec, we utilize CR \mathcal{R}_{θ_R} built upon MLP to model the distribution as follows:

$$p_{\mathbf{v} \sim p(\mathcal{M}^v), \boldsymbol{\eta} \sim p(\mathcal{M}^{v \rightarrow i}, \mathcal{M}^{v \rightarrow t}, \mathcal{M}^v)}(\mathbf{x} | \mathbf{v}, \boldsymbol{\eta}), \quad (10)$$

$$\begin{aligned} \hat{\mathcal{M}}_d^v &= \mathcal{R}_{\theta_R}(\mathcal{M}^v, \boldsymbol{\eta}_{\{v, i, t\}}) \\ &= \gamma(\boldsymbol{\eta}^{(j)}) \odot \tau_j + \beta(\boldsymbol{\eta}^{(j)}), \quad \boldsymbol{\eta}^{(j)} \in \boldsymbol{\eta}_{\{v, i, t\}}, \end{aligned} \quad (11)$$

where τ_j is the activation of j -th layer, γ and β are affine layers, and \odot is the Hadamard product.

In VVTRec, the set of unfrozen trainable parameters Θ comprises $\theta_{c,1}, \theta_{c,2}, \theta_v, \theta_R$, ensuring that no excessive computational overhead is introduced. Thus, VVTRec is optimized by utilizing losses computed from complex values in the frequency domain [Jiang *et al.*, 2021]:

$$\min_{\Theta} \mathcal{L}(\hat{\mathcal{M}}_d^v, \mathcal{M}_d^v) = \text{Avg} \left(\omega \left| \hat{\mathcal{M}}_d^v - \mathcal{M}_d^v \right|^2 \right), \quad (12)$$

$$\omega = \left(\frac{\rho}{\max(\rho)} + 1 \right) \left| \hat{\mathcal{M}}_d^v - \mathcal{M}_d^v \right|, \quad (13)$$

where \mathcal{M}_d^v is the ground truth, Avg denotes the average operation on the uv-plane, ρ denotes the amplitude.

4 Experiments

4.1 Experimental Setup

Following the latest methods [Wang *et al.*, 2024], we utilize a consistent telescope configuration to sample visibility data using the eht-imaging toolkit [Chael *et al.*, 2018; Chael *et al.*, 2019] from real astronomical observations in different public datasets of distinct galaxy morphologies: Merging Galaxies (MG), In-between Round Smooth Galaxies (IRSG), Unbarred Tight Spiral Galaxies (UTSG), and Edge-on Galaxies with Bulge (EGB). These data are collected from

the DESI Legacy Imaging Surveys [Dey *et al.*, 2019], integrating contributions from the Beijing-Arizona Sky Survey (BASS) [Zou *et al.*, 2017], the DECam Legacy Survey (DECaLS) [Blum *et al.*, 2016], and the Mayall z-band Legacy Survey [Silva *et al.*, 2016]. The parameters for observation are adjusted to mirror an 8-telescope Event Horizon Telescope (EHT) setup to ensure consistency. We conduct experiments by utilizing the PyTorch [Paszke *et al.*, 2019] framework on an NVIDIA H800 GPU. To quantitatively analyze the quality of reconstructions, we adopt two commonly used metrics, Peak Signal-to-Noise Ratio (PSNR) and Structural Similarity Index Measure (SSIM), for evaluating the generated images.

4.2 Overall Comparison

As shown in Table 1, VVTRec outperforms previous methods across datasets. The best results of PSNR and SSIM are highlighted in bold, respectively. The second-best results are underlined. Overall, the average PSNR of VVTRec is 1.909 higher than the second best on four datasets. Compared with traditional methods, we can obtain an average improvement of 8.199. Such performance gains strongly show that our multimodal advancements on visibility can really contribute to the underlying feature extractions of weak signals and enhanced reconstruction. Meanwhile, improvements in SSIM show that VVTRec indeed better integrates the pre-trained knowledge with original astronomical significance to produce reconstructions with more plausible image structures than unimodal methods. This improvement enhances the reliability for astronomical research, as structural information about celestial objects often provides useful insights.

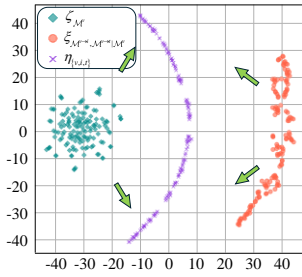
We further demonstrate the dirty image, reconstruction results of VVTRec and real sky, including both visibility and image in Figure 5. We can observe abundant artifacts in dirty

Table 1: **Comparison results on different datasets using the full training set.** The Peak Signal to Noise Ratio (PSNR↑: higher is better) and Structural Similarity Index Measure (SSIM↑) are reported. **Bold** and underlined denote the best and second best results respectively.

Method	Type	MG		IRSG		UTSG		EGB	
		PSNR↑	SSIM↑	PSNR↑	SSIM↑	PSNR↑	SSIM↑	PSNR↑	SSIM↑
DIRTY [Gilbert <i>et al.</i> , 2014]	Traditional	11.633	0.715	11.398	0.722	11.890	0.725	11.356	0.708
CLEAN [Cornwell, 2008]	Traditional	18.557	0.818	20.913	0.839	17.048	0.806	19.448	0.831
U-Net [Xie and Li, 2022]	Unimodal	18.126	0.818	19.770	0.828	14.877	0.786	19.232	0.822
Radionets [Schmidt <i>et al.</i> , 2022]	Unimodal	19.687	0.836	21.369	0.854	20.828	0.844	20.322	0.836
NF [Wu <i>et al.</i> , 2022]	Unimodal	20.560	0.875	24.099	0.898	21.323	0.880	21.276	0.879
VisRec [Wang <i>et al.</i> , 2025]	Unimodal	22.267	0.883	24.940	0.915	23.805	0.909	23.268	0.901
PolarRec [Wang <i>et al.</i> , 2024]	Unimodal	24.088	0.884	26.234	0.912	25.384	0.904	25.420	0.908
VVTRec(Ours)	Multimodal	26.164	0.919	28.276	0.932	27.261	0.928	27.061	0.924

Table 2: **Computational and reconstruction performance comparisons of VVTRec using different pre-trained models.** **Bold** and underlined denote the best and second best results respectively.

Model	Number (M) / Memory (MiB) of Learnable Parameters	Speed (s/iter)	MG		IRSG		UTSG		EGB	
			PSNR↑	SSIM↑	PSNR↑	SSIM↑	PSNR↑	SSIM↑	PSNR↑	SSIM↑
PolarRec	14.9 / 59.7	0.0094	24.088	0.884	26.234	0.912	25.384	0.904	25.420	0.908
VVTRec+ViLT	17.6 / 70.2	0.0158	25.747	0.917	28.134	0.931	27.192	0.927	26.764	0.923
VVTRec+CLIP	17.5 / 69.9	0.0138	26.164	<u>0.919</u>	<u>28.276</u>	<u>0.932</u>	27.261	0.928	<u>27.061</u>	<u>0.924</u>
VVTRec+BLIP	18.0 / 72.1	0.0623	26.139	<u>0.920</u>	28.363	<u>0.933</u>	27.242	<u>0.929</u>	27.063	<u>0.925</u>



Statistic	$\zeta_{\mathcal{M}^v}$	$\xi_{\mathcal{M}^v \rightarrow i, \mathcal{M}^v \rightarrow t \mathcal{M}^v}$	$\eta_{\{v,i,t\}}$
Mean ¹	-44.109	57.357	3.242
SD ²	10.309	14.924	15.055
Entropy	6.844	6.433	6.458

¹Calculated from 1D t-SNE

²SD stands for Standard Deviation

Figure 6: t-SNE visualization of the key latent components involved in the modelling of the multimodal joint representation and illustrations of their corresponding statistics.

images. VVTRec successfully reconstructs and preserves various features with different shapes of celestial objects, addressing the issue of unrealistic reconstructions caused by the point-like sources assumption. It effectively removes artifacts and noise, better supporting subsequent scientific studies.

4.3 Applicability and Computational Cost

To demonstrate the applicability of VVTRec, we conduct extended experiments on four datasets with three representative pre-trained VLMs, namely ViLT [Kim *et al.*, 2021], CLIP [Radford *et al.*, 2021], and BLIP [Li *et al.*, 2023; Xue *et al.*, 2025] to show that boosting performances by expanding modalities in VVTRec does not necessarily introduce excessive computational overhead, as shown in Table 2. Specifically, VVTRec+CLIP and VVTRec+BLIP typically gain the best and second-best results across datasets. This performance demonstrates that VVTRec can better utilize profound pre-trained knowledge. Among the three models, VVTRec+CLIP has the fewest learnable parameters. Compared with the unimodal method PolarRec, the number of learnable parameters is only 2.6 M higher, while the memory

consumption is only 10.2 MiB higher. In terms of the training speed, VVTRec+CLIP surpasses the other two models, making it the best one balancing performance and training resources. In summary, these models all outperform previous methods, demonstrating the effectiveness and applicability of our framework. It shows that VVTRec can handle different cases of distinct VLMs providing external knowledge, and thereby aid in exploiting visibility modality deeply.

4.4 Qualitative Analysis of Multimodal Features

In this experiment, we visualize the key latent components $\zeta_{\mathcal{M}^v}$, $\xi_{\mathcal{M}^v \rightarrow i, \mathcal{M}^v \rightarrow t | \mathcal{M}^v}$, and $\eta_{\{v,i,t\}}$ to show the effective establishment of multimodal features. We utilize the t-distributed Stochastic Neighbor Embedding (t-SNE) [Maaten and Hinton, 2008] to map the high-dimensional latent embeddings into a two-dimensional space as shown in Figure 6. We also calculate several statistics to facilitate quantitative analysis. Specifically, we conduct 1D t-SNE analysis to obtain the mean values in \mathbb{R}^1 . Observing mean values, the multimodal feature $\eta_{\{v,i,t\}}$ lies between the other two features, indicating the information fusion between the query and knowledge. Furthermore, the standard deviation of $\eta_{\{v,i,t\}}$ is higher than that of the other two features, indicating an increased intra-class variance. Additionally, comparisons of entropy demonstrate that $\eta_{\{v,i,t\}}$ has retained information content from both sources successfully. Qualitatively, the multimodal features in the 2D space are positioned between the other two, preserving the ring-like characteristics of $\zeta_{\mathcal{M}^v}$ while also capturing the elongated features of $\xi_{\mathcal{M}^v \rightarrow i, \mathcal{M}^v \rightarrow t | \mathcal{M}^v}$. This phenomenon demonstrates that the information extraction from $\xi_{\mathcal{M}^v \rightarrow i, \mathcal{M}^v \rightarrow t | \mathcal{M}^v}$ by $\zeta_{\mathcal{M}^v}$ in VVTRec is effective.

4.5 Data-Efficient Analysis

A data-efficient reconstruction method is particularly meaningful for astronomy, whose data acquisition through tele-

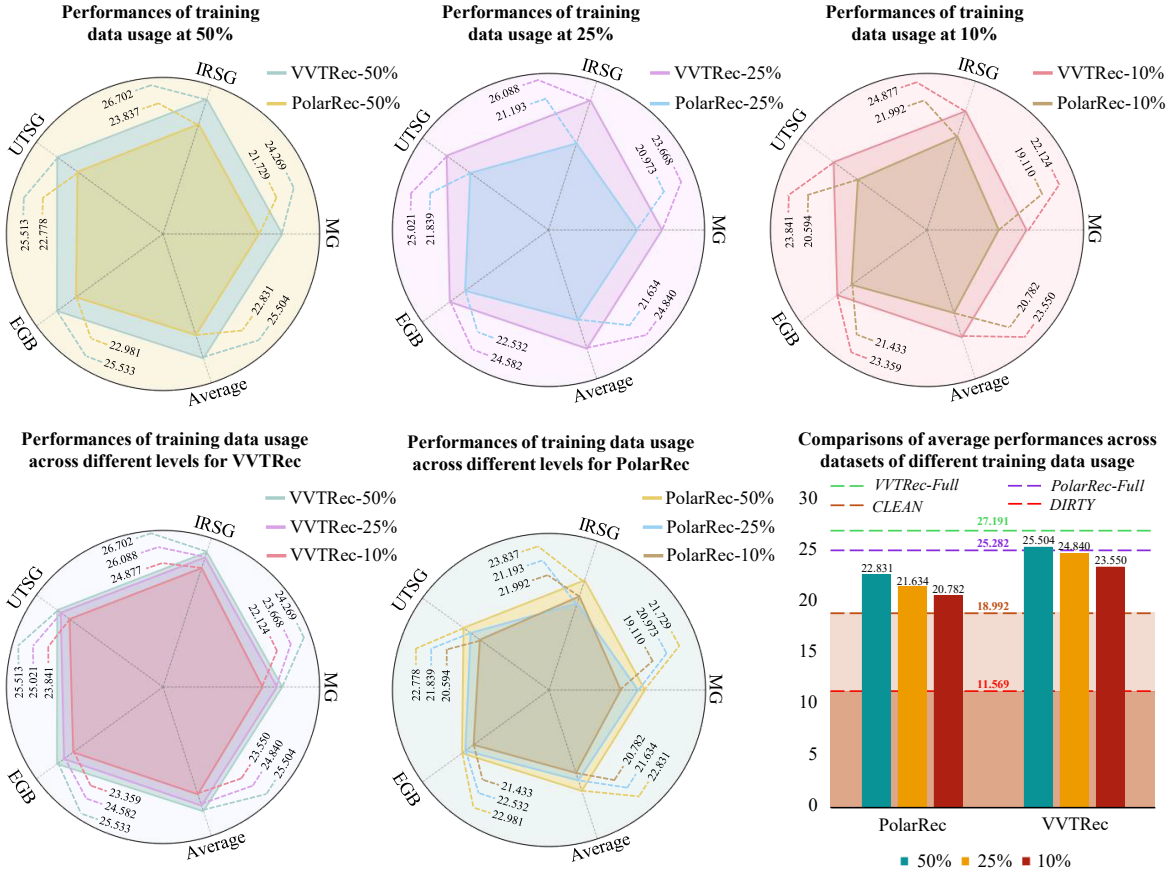


Figure 7: Radar plots comparing the PSNR results on the full test set with 10%, 25%, and 50% training data usage between VVTRec and PolarRec. The bar chart further shows comparisons of results between data-efficient training and full data usage training.

scopes is expensive, challenging, and labor-intensive [Kruk *et al.*, 2023]. We further conduct experiments of utilizing portions of training data but testing on the full test set to show the data efficiency of VVTRec. We choose the best unimodal method, PolarRec, as the comparison. Specifically, we first illustrate the PSNR comparisons on the full test set between VVTRec and PolarRec with 10%, 25%, and 50% training data usage in the first row of Figure 7, respectively. Higher values (larger radius) indicate better performance. We find that VVTRec consistently outperforms PolarRec. Then, we also compare the performance of VVTRec-10%, -25%, and -50% in the first radar plot of the second row. The second radar plot of the second row illustrates similar content for PolarRec. It shows that the decrease in available training data causes a smaller impact on VVTRec than PolarRec since areas shrink faster in PolarRec. At last, we show the average performance comparisons across datasets between our data-efficient training and baselines of full data usage in a bar chart. It shows that the performance of VVTRec-10% can still surpass PolarRec-50% even though 40% more data has been removed. Finally, VVTRec-50% can obtain a comparable performance with PolarRec-Full, achieving the best performance compared to unimodal methods. Overall, experimental results showcase the data efficiency of VVTRec in potential cases of scarce astronomical data.

5 Conclusion and Future Work

This work develops a multimodal radio interferometric data reconstruction method with visibility-guided visual and textual modality enrichment, called VVTRec. It can transform sparse visibility into expanded modalities and integrate external knowledge in a sample-specific manner to tackle the current challenges in visibility data reconstruction: (1) weak astronomical signals with insufficient reconstruction knowledge, and (2) the difficulty in supplementing knowledge for unimodal methods due to visibility data being a foreign modality. Extensive experimental results demonstrate superior performance across multiple datasets without introducing excessive computational overhead, showcasing the effectiveness of our approach. Our work provides a foundation for multimodal interferometric data reconstruction. Findings have the potential to extend beyond the immediate scope of radio astronomy. Given our method’s ability to efficiently transform domain-specific features into enriched multimodal features, it holds substantial promise for deployment in other cross-disciplinary scenarios. Specifically, we envision its application in fields such as magnetic resonance imaging, as well as in seismic imaging. Future work could also involve exploring these avenues to demonstrate the versatility of our approach.

References

[Ables, 1974] JG Ables. Maximum entropy spectral analysis. *Astronomy and Astrophysics Supplement*, Vol. 15, p. 383, 15:383, 1974.

[Blum *et al.*, 2016] Robert D Blum, Kaylan Burleigh, Arjun Dey, David J Schlegel, Aaron M Meisner, Michael Levi, Adam D Myers, Dustin Lang, John Moustakas, Anna Patej, et al. The decam legacy survey. In *American Astronomical Society Meeting Abstracts# 228*, volume 228, pages 317–01, 2016.

[Bouman *et al.*, 2016] Katherine L Bouman, Michael D Johnson, Daniel Zoran, Vincent L Fish, Sheperd S Doeleman, and William T Freeman. Computational imaging for VLBI image reconstruction. In *Proceedings of the IEEE Conference on Computer Vision and Pattern Recognition*, pages 913–922, 2016.

[Bouman *et al.*, 2018] Katherine L Bouman, Michael D Johnson, Adrian V Dalca, Andrew A Chael, Freek Roelofs, Sheperd S Doeleman, and William T Freeman. Reconstructing video of time-varying sources from radio interferometric measurements. *IEEE Transactions on Computational Imaging*, 4(4):512–527, 2018.

[Chael *et al.*, 2018] Andrew A Chael, Michael D Johnson, Katherine L Bouman, Lindy L Blackburn, Kazunori Akiyama, and Ramesh Narayan. Interferometric imaging directly with closure phases and closure amplitudes. *The Astrophysical Journal*, 857(1):23, 2018.

[Chael *et al.*, 2019] Andrew A Chael, Katherine L Bouman, Michael D Johnson, Ramesh Narayan, Sheperd S Doeleman, John FC Wardle, Lindy L Blackburn, Kazunori Akiyama, Maciek Wielgus, Chi-kwan Chan, et al. ehtim: Imaging, analysis, and simulation software for radio interferometry. *Astrophysics Source Code Library*, pages ascl-1904, 2019.

[Collaboration *et al.*, 2022] Chime/Frb Collaboration, Bridget C Andersen, Kevin Bandura, Mohit Bhardwaj, PJ Boyle, Charanjot Brar, Daniela Breitman, Tomas Cassanelli, Shami Chatterjee, Pragya Chawla, et al. Sub-second periodicity in a fast radio burst. *Nature*, 607(7918):256–259, 2022.

[Connor *et al.*, 2022] Liam Connor, Katherine L Bouman, Vikram Ravi, and Gregg Hallinan. Deep radio-interferometric imaging with POLISH: DSA-2000 and weak lensing. *Monthly Notices of the Royal Astronomical Society*, 514(2):2614–2626, 2022.

[Cornwell, 2008] Tim J Cornwell. Multiscale CLEAN deconvolution of radio synthesis images. *IEEE Journal of Selected Topics in Signal Processing*, 2(5):793–801, 2008.

[Dey *et al.*, 2019] Arjun Dey, David J Schlegel, Dustin Lang, Robert Blum, Kaylan Burleigh, Xiaohui Fan, Joseph R Findlay, Doug Finkbeiner, David Herrera, Stéphanie Juneau, et al. Overview of the DESI legacy imaging surveys. *The Astronomical Journal*, 157(5):168, 2019.

[Gilbert *et al.*, 2014] Anna C Gilbert, Piotr Indyk, Mark Iwen, and Ludwig Schmidt. Recent developments in the sparse Fourier transform: A compressed Fourier transform for big data. *IEEE Signal Processing Magazine*, 31(5):91–100, 2014.

[Högbom, 1974] JA Högbom. Aperture synthesis with a non-regular distribution of interferometer baselines. *Astronomy and Astrophysics Supplement*, Vol. 15, p. 417, 15:417, 1974.

[Jiang *et al.*, 2021] Liming Jiang, Bo Dai, Wayne Wu, and Chen Change Loy. Focal frequency loss for image reconstruction and synthesis. In *Proceedings of the IEEE/CVF International Conference on Computer Vision*, pages 13919–13929, 2021.

[Jin *et al.*, 2025] Zikun Jin, Yuhua Qian, Xinyan Liang, and Haijun Geng. A multi-view fusion approach for enhancing speech signals via short-time fractional fourier transform. In *Proceedings of the International Joint Conference on Artificial Intelligence*, pages 5508–5516, 2025.

[Kim *et al.*, 2021] Wonjae Kim, Bokyung Son, and Ildoo Kim. ViLT: Vision-and-language transformer without convolution or region supervision. In *International Conference on Machine Learning*, pages 5583–5594. PMLR, 2021.

[Kruk *et al.*, 2023] Sandor Kruk, Pablo García-Martín, Marcel Popescu, Ben Aussel, Steven Dillmann, Megan E Perks, Tamina Lund, Bruno Merín, Ross Thomson, Samet Karadag, et al. The impact of satellite trails on Hubble Space Telescope observations. *Nature Astronomy*, 7(3):262–268, 2023.

[Li *et al.*, 2023] Junnan Li, Dongxu Li, Silvio Savarese, and Steven Hoi. BLIP-2: Bootstrapping language-image pre-training with frozen image encoders and large language models. In *International Conference on Machine Learning*, pages 19730–19742. PMLR, 2023.

[Lin *et al.*, 2014] Tsung-Yi Lin, Michael Maire, Serge Belongie, James Hays, Pietro Perona, Deva Ramanan, Piotr Dollár, and C Lawrence Zitnick. Microsoft coco: Common objects in context. In *European Conference on Computer Vision*, pages 740–755. Springer, 2014.

[Maaten and Hinton, 2008] Laurens van der Maaten and Geoffrey Hinton. Visualizing data using t-sne. *Journal of Machine Learning Research*, 9(Nov):2579–2605, 2008.

[Paszke *et al.*, 2019] Adam Paszke, Sam Gross, Francisco Massa, Adam Lerer, James Bradbury, Gregory Chanan, Trevor Killeen, Zeming Lin, Natalia Gimelshein, Luca Antiga, et al. Pytorch: An imperative style, high-performance deep learning library. *Advances in Neural Information Processing Systems*, 32, 2019.

[Radford *et al.*, 2021] Alec Radford, Jong Wook Kim, Chris Hallacy, Aditya Ramesh, Gabriel Goh, Sandhini Agarwal, Girish Sastry, Amanda Askell, Pamela Mishkin, Jack Clark, et al. Learning transferable visual models from natural language supervision. In *International Conference on Machine Learning*, pages 8748–8763. PMLR, 2021.

[Schmidt *et al.*, 2022] Kevin Schmidt, Felix Geyer, Stefan Fröse, P-S Blomenkamp, Marcus Brüggen, Francesco

De Gasperin, Dominik Elsässer, and Wolfgang Rhode. Deep learning-based imaging in radio interferometry. *Astronomy & Astrophysics*, 664:A134, 2022.

[Silva *et al.*, 2016] David R Silva, Robert D Blum, Lori Allen, Arjun Dey, David J Schlegel, Dustin Lang, John Moustakas, Aaron M Meisner, Francisco Valdes, Anna Patej, et al. The mayall z-band legacy survey. In *American Astronomical Society Meeting Abstracts# 228*, volume 228, pages 317–02, 2016.

[Singh *et al.*, 2022] Saurabh Singh, Jishnu Nambissan T, Ravi Subrahmanyam, N Udaya Shankar, BS Girish, A Raghunathan, R Somashekhar, KS Srivani, and Mayuri Sathyaranayana Rao. On the detection of a cosmic dawn signal in the radio background. *Nature Astronomy*, 6(5):607–617, 2022.

[Steyn *et al.*, 2024] Nadia Steyn, Renée C Kraan-Korteweg, Sambatriniaina HA Rajohnson, Sushma Kurapati, Hao Chen, Bradley Frank, Paolo Serra, Lister Staveley-Smith, Fernando Camilo, and Sharmila Goedhart. H i galaxy signatures in the SARAO MeerKAT Galactic Plane Survey—I. Probing the richness of the great attractor wall across the inner zone of avoidance. *Monthly Notices of the Royal Astronomical Society: Letters*, 529(1):L88–L94, 2024.

[Thompson *et al.*, 2017] A Richard Thompson, James M Moran, and George W Swenson. *Interferometry and synthesis in radio astronomy*. Springer Nature, 2017.

[Vaswani *et al.*, 2017] Ashish Vaswani, Noam Shazeer, Niki Parmar, Jakob Uszkoreit, Llion Jones, Aidan N Gomez, Łukasz Kaiser, and Illia Polosukhin. Attention is all you need. *Advances in Neural Information Processing Systems*, 30, 2017.

[Wang *et al.*, 2023] Ruoqi Wang, Zhuoyang Chen, Qiong Luo, and Feng Wang. A conditional denoising diffusion probabilistic model for radio interferometric image reconstruction. In *European Conference on Artificial Intelligence*, volume 372, pages 2499–2506, 2023.

[Wang *et al.*, 2024] Ruoqi Wang, Zhuoyang Chen, Jiayi Zhu, Qiong Luo, and Feng Wang. PolarRec: Improving radio interferometric data reconstruction using polar coordinates. In *Proceedings of the IEEE/CVF Conference on Computer Vision and Pattern Recognition*, pages 12841–12850, 2024.

[Wang *et al.*, 2025] Ruoqi Wang, Haitao Wang, Qiong Luo, Feng Wang, and Hejun Wu. VisRec: A semi-supervised approach to visibility data reconstruction in radio astronomy. In *Proceedings of the AAAI Conference on Artificial Intelligence*, volume 39, pages 852–860, 2025.

[Wilson, 1979] Robert W Wilson. The cosmic microwave background radiation. *Science*, 205(4409):866–874, 1979.

[Wu *et al.*, 2022] Benjamin Wu, Chao Liu, Benjamin Eckart, and Jan Kautz. Neural interferometry: Image reconstruction from astronomical interferometers using transformer-conditioned neural fields. In *Proceedings of the AAAI Conference on Artificial Intelligence*, pages 2685–2693, 2022.

[Xie and Li, 2022] Yutong Xie and Quanzheng Li. Measurement-conditioned denoising diffusion probabilistic model for under-sampled medical image reconstruction. In *International Conference on Medical Image Computing and Computer-Assisted Intervention*, pages 655–664. Springer, 2022.

[Xu *et al.*, 2022] CK Xu, C Cheng, PN Appleton, P-A Duc, Y Gao, N-Y Tang, M Yun, YS Dai, J-S Huang, U Lisenfeld, et al. A 0.6 Mpc H i structure associated with Stephan’s Quintet. *Nature*, 610(7932):461–466, 2022.

[Xue *et al.*, 2025] Le Xue, Manli Shu, Anas Awadalla, Jun Wang, An Yan, Senthil Purushwalkam, Honglu Zhou, Vibraj Prabhu, Yutong Dai, Michael S Ryoo, et al. BLIP-3: A family of open large multimodal models. In *Proceedings of the IEEE/CVF International Conference on Computer Vision*, pages 6124–6135, 2025.

[Zhang *et al.*, 2025] Jianke Zhang, Yanjiang Guo, Yucheng Hu, Xiaoyu Chen, Xiang Zhu, and Jianyu Chen. UP-VLA: A unified understanding and prediction model for embodied agent. In *International Conference on Machine Learning*, 2025.

[Zhao *et al.*, 2025a] Wei Zhao, Pengxiang Ding, Min Zhang, Zhefei Gong, Shuanghao Bai, Han Zhao, and Donglin Wang. VLAS: Vision-language-action model with speech instructions for customized robot manipulation. In *International Conference on Learning Representations*, 2025.

[Zhao *et al.*, 2025b] Xu Zhao, Ren Liu, and Weiran Shen. Public signaling in markets with information asymmetry using a limited number of signals. In *Proceedings of the International Joint Conference on Artificial Intelligence*, pages 4091–4099, 2025.

[Zhong *et al.*, 2025] Siru Zhong, Weilin Ruan, Ming Jin, Huan Li, Qingsong Wen, and Yuxuan Liang. Time-VLM: Exploring multimodal vision-language models for augmented time series forecasting. In *International Conference on Machine Learning*, 2025.

[Zou *et al.*, 2017] Hu Zou, Xu Zhou, Xiaohui Fan, Tianmeng Zhang, Zhimin Zhou, Jundan Nie, Xiyan Peng, Ian McGreer, Linhua Jiang, Arjun Dey, et al. Project overview of the beijing–arizona sky survey. *Publications of the Astronomical Society of the Pacific*, 129(976):064101, 2017.